Fast and Accurate Thermal Modeling of Magnetic Components by FEA-Based Homogenization

Guillermo Salinas López, Alberto Delgado Expósito, Javier Muñoz-Antón, Jesús Ángel Oliver Ramírez, and Roberto Prieto López

***Abstract*—The use of three-dimensional (3D) thermal simulations of magnetic components for power converters is limited to validation of final designs due to time consumption. A two-step homogenization is proposed to simplify them, while keeping good accuracy. The required equations and some guidelines are described in this paper. It can be applied to solid round wire, litz wire, or foil wound magnetic components. Considerations to extend its use to transformers, including the use of interleaving techniques and insulating tape, are explained. This method can reduce the computation time of 3-D simulations (seven times faster than usual simulations) while the convergence is assured even for complex structures or cases with litz wire. Finally, the method is experimentally validated with DC and AC excitation.**

***Index Terms*—Electrothermal effects, inductors, power transformer thermal factors, transformers.**

NOMENCLATURE

a, b, c, d	Coefficients for the proposed multivariable fitting.
A_{cond}	Area of conductor.
A_{ins}	Area of insulation.
AWG	American wire gauge.
h	Heat transfer coefficient or film coefficient.
k	Thermal conductivity.
k_a	Thermal conductivity of surrounding material (air, potting).
k_{cond}	Thermal conductivity of conductor material.
k_{eq}	Effective thermal conductivity.
$k_{\text{eq}_{\text{ort}}}$	Effective thermal conductivity in the orthogonal direction.
k_{eq_r}	Effective thermal conductivity in the radial direction.
k_{eq_θ}	Effective thermal conductivity in the angular direction.
$k_{\text{eq}_{\text{tan}}}$	Effective thermal conductivity in the tangential direction.
$k_{\text{eq}_{\text{TOT}}}$	Effective thermal conductivity of several homogenized blocks.
k_{eq_z}	Effective thermal conductivity in the vertical direction.
k_{fe}	Thermal conductivity of ferrite.
k_i	Thermal conductivity of wire insulation.
k_i'	Homogenized thermal conductivity of different insulation.
$k_{i_{\text{bund}}}$	Thermal conductivity of bundle impregnation.
$k_{i_{\text{imp}}}$	Thermal conductivity of wire impregnation.
$k_{i_{\text{st}}}$	Thermal conductivity of strand insulation.
k_{ins}	Thermal conductivity of insulation layers.
k_{ratio}	Thermal conductivity ratio (k_w/k_a).
k_w	Thermal conductivity of a homogenized wire.
l_{cond}	Width of conductors.
l_{ins}	Width of insulation layers.
n_{cond}	Number of conductor layers.
n_{ins}	Number of insulation layers.
N_{layers}	Total number of layers.
PF	Packing factor of a litz bundle.
P_{pri}	Losses in primary winding.
P_{sec}	Losses in secondary winding.
q''	Heat flux.
q_x''	Heat flux in the *x* direction.
r_1	Inner radius of a cylindrical foil winding.
r_n	Radius of the *n* foil layer.
r_{crit}	Critical radius.
τ	Volume fraction of conductor material.
τ^*	Introduced variable to replace τ.
$T_{c_{\text{max}}}$	Maximum core temperature.
$T_{c_{\text{surf}}}$	Average core surface temperature.
$T_{w_{\text{max}}}$	Maximum winding temperature.
$T_{w_{\text{surf}}}$	Average winding surface temperature.
ΔT	Temperature rise.
ΔT_{exp}	Measured temperature rise.
$\Delta T_{(\text{wireFEA})}$	Temperature rise with "wire-level" homogenization.
ΔT_{sim}	Temperature rise obtained by simulation.
$\Delta T_{(\text{windFEA})}$	Temperature rise with "winding-level" homogenization.
ϕ	Wire diameter.

Manuscript received December 17, 2018; revised April 27, 2019; accepted May 31, 2019. Date of publication June 4, 2019; date of current version November 12, 2019. The work of G. Salinas was supported by the "Universidad Politécnica de Madrid," (predoctoral Contract RD99/2011) under Grant *"Programa Propio."* Recommended for publication by Associate Editor H. Wang. This paper was presented in part at the Energy Conversion Congress and Exposition, Portland, OR, USA, September 2018. *(Corresponding author: Guillermo Salinas López.)*

G. Salinas López, A. Delgado Expósito, J. Á. Oliver Ramírez, and R. Prieto López are with the Centro de Electrónica Industrial, Universidad Politécnica de Madrid, Madrid 28006, Spain (e-mail: guillermo.salinas@upm.es; a.delgado@upm.es; jesusangel.oliver@upm.es; roberto.prieto@upm.es).

J. Muñoz-Antón is with the Grupo de Investigaciones Termoenergéticas, Universidad Politécnica de Madrid, Madrid 28006, Spain (e-mail: jamunoz@etsii.upm.es).

Color versions of one or more of the figures in this paper are available online at http://ieeexplore.ieee.org.

Digital Object Identifier 10.1109/TPEL.2019.2921160

v_{cond}	Volume of conductor material.
$v_{i_{\text{st}}}$	Volume of strand insulation material.
$v_{i_{\text{imp}}}$	Volume of impregnation material.
$v_{i_{\text{bund}}}$	Volume of bundle insulation.
v_w	Volume of a wire.
w	Width of the cell under study.

I. Introduction

DUE to the interdependence between electromagnetic (EM) and thermal fields, proper modeling of both domains is needed to optimize magnetic components for power converters. As a result, a good accuracy of the thermal models is required to get better optimized magnetic components, with higher power density and lower size, while ensuring their operation below the thermal limit.

Some analytic solutions to estimate the temperature of the magnetic components can be found in the literature. Manufacturers usually provide empirical equations for each core shape [1], [2]. A simple equation was introduced in [3] for any core shape and size. These approaches are useful as first-order approximations during the early design iterations, but its use in optimization processes would lead to non-optimized designs. Another empirical model for potted litz wound toroid inductors is developed in [4], while it offers a good accuracy, its use is limited to the shape of the component, the winding arrangement, and the boundary conditions (no convection, since that model is developed for space environment conditions) used in their experimental setup.

Another approach to solve the thermal problem is the use of one-dimensional (1D) models' thermal networks. In [5], a 1-D thermal network is proposed to consider the heat transfer path from the center core leg of a magnetic component to the top and bottom core parts by means of parallel thermal resistors. The effect of convection and radiation inside the window is also modeled in [6]. Some details are added compared to [5] and avoid simplifying the radiation, but the heat transfer in other directions is neglected, what might infer a high error in the temperature estimation.

The most accurate solutions are achieved by means of 3-D FEA simulations. The downside is that they are substantially time-consuming, due to the mesh requirements of the conductors, specially in the case of litz wires. Additionally, if the mesh is too demanding, such as detailed simulations of litz wire windings, 3-D simulations might become unfeasible.

Homogenization techniques have been traditionally used to simplify either the mathematical analysis or the simulations in different physics fields, which consist in replacing heterogeneous systems by a single component whose calculated properties make it macroscopically behave as the original system. In thermal analysis, that property is the effective thermal conductivity k_{eq} from the heat equation $\vec{q''} = -k\vec{\nabla}T$ [7], [8]. A review of the traditional analytic models to obtain k_{eq} is detailed in [9]. Some of these methods are used in [10] to get the effective conductivity of bundles of litz wire for electrical machines.

In this paper, one step further is carried out and the homogenization is applied at two levels. The first one, described in Section II-A, includes the conductor and its insulation. The latter is applied at winding level, where the wires and the material between them (air or potting resin) are homogenized, explained in Section II-B. An application example is depicted in Fig. 1.

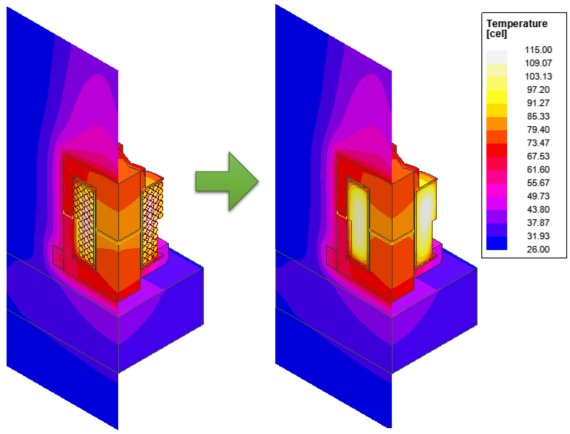

Fig. 1. 3-D thermal distribution on a cut plane of a PQ core inductor: detailed FEA simulation (left); homogenized winding (right).

The main features of the proposed method are as follows:

1) Simplified thermal analysis of the winding while keeping a good accuracy, since the equations are based on FEA results.
2) Reduction of the running time of 3-D thermal simulations by a factor between 6 and 8, compared with detailed simulations, due to the resulting simpler mesh.
3) Assured convergence of 3-D thermal simulations, which allows the analysis of complex problems.

This two-level homogenization for magnetic components was introduced in [11]. A simplification of the set of equations and some explanations to extend this approach to model inductors and transformers with any winding type are presented in this paper.

The paper is structured as follows. In Section II, the concept is described. It involves a two-step homogenization. The first step is at a wire level, explained in Section II-A for round solid wires and litz bundles, with round or square section. Afterward, the second step is applied at a winding level, for round solid or litz, square litz, and foil winding. It is described in Section II-B. Then, the application of the two-level homogenization for transformers is particularized in Section III, in which some especial concern needs to be considered if an interleaving technique or insulation between layers is used. In Section IV the method is experimentally validated with DC and AC excitation and the reduction of the simulation time for 3-D FEA is analyzed. Finally, conclusions are presented in Section V.

II. Method: Two-Level Homogenization

The proposed two-stage homogenization is described in this section. The first step, described in Section II-A, comprehends the conductor and its insulation. The latter, explained in Section II-B, is applied at the winding level, where the wires and the material between them (air or potting resin) are homogenized. Fig. 2 shows a diagram of the method.

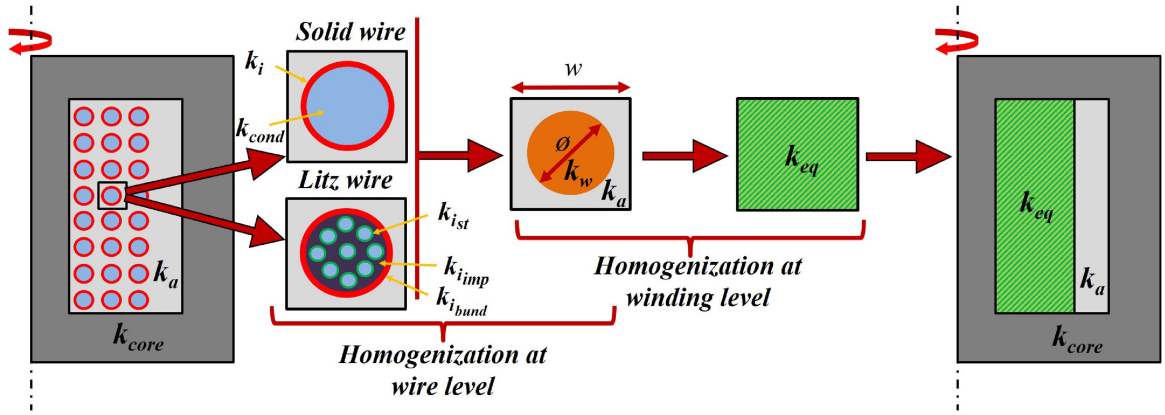

Fig. 2. Design flow to model the winding thermal equivalent layer (pot core is used as an illustrative example). From left to right: cross-sectional area of a pot core inductor, as an example; homogenization at wire level and at winding level; inductor with the equivalent layer.

A. Wire-Level Homogenization

The first step is to homogenize the conductor and insulation materials. The process to homogenize different conductor types (round solid wire, round and square litz) for any magnetic component is discussed along the following sections.

1) Round Solid Wire: In this case, there is no homogenization strictly speaking. Nevertheless, a simplification is required in order to avoid an excessively restrictive mesh of the wires: its insulation should be neglected. This simplification does not compromise the temperature estimation since the temperature gradient within a conductor and in the insulator is negligible. The reasons for this are the reduced dimensions of the wire, the high thermal conductivity of the conductor, and its internal heat generation. This assumption is valid for commercial wires lower than AWG 10 (external diameter of 2.59 mm) [7], used for low and medium power applications (< 100 kW).

In addition, since the insulator thickness of common commercial solid wires is below the *critical radius* value ($r_{\text{crit}} = k_i/h = 0.04\ \text{W/m}\cdot\text{K}/5\ \text{W/m}^2\cdot\text{K} = 8\ (\text{mm})$ for common operating conditions) [7], [8], it is reasonable to consider that the effective thermal conductivity of the whole wire is equal to the conductor material conductivity ($k_w = k_{\text{cond}}$). More details regarding the *critical radius* can be found in [7] and [8].

Furthermore, the thermal conductivity has a dependence on temperature. However, the conductivity of copper and aluminum wires can be assumed constant and equal to $401\ \text{W/m}\cdot\text{K}$ and 237 W/m· K, respectively, for a temperature range between 0 °C and 100 °C [12].

2) Litz Wire With Round or Square Section: This is another usual case. Due to the high number of strands within a litz bundle and their reduced diameter, the homogenization of the bundle is required to make possible its thermal analysis. Different methods are discussed next.

It is important to distinguish between two different types of litz wire: impregnated (the strands from a bundle are embedded within a potting material) and non-impregnated (no potting is used in the bundle). A study in [13] reveals that Hashin–Shtrikman's method for two-phase composite materials [14] is more suitable for impregnated ones—a comparison with experimental results is provided in that paper to validate this statement—for which the thermal properties of the impregnation and insulation materials are close and might be considered equal. Then, the conductivity of the bundle k_w can be described as

$$k_w = k_i \cdot \frac{(1+\tau)\cdot k_{\text{cond}} + (1-\tau)\cdot k_i}{(1-\tau)\cdot k_{\text{cond}} + (1+\tau)\cdot k_i} \tag{1}$$

where k_{cond} is the conductor strand conductivity, k_i is the insulator conductivity, and τ is the volume fraction of conductor material ($\tau = \text{vol}_{\text{cond}}/\text{vol}_{\text{tot}}$). However, the error due to the previous assumption might be unacceptable if the impregnation and insulation materials's properties cannot be assumed as equal. In [15], the use of k_i' instead of k_i in (1) to account for the different conductivity of the insulator (i_{st} subscript) and impregnation (i_{imp}) materials. The definition of k_i' is

$$k_i' = \frac{k_{i_{\text{st}}}\cdot v_{i_{\text{st}}} + k_{i_{\text{imp}}}\cdot v_{i_{\text{imp}}} + k_{i_{\text{bund}}}\cdot v_{i_{\text{bund}}}}{v_{i_{\text{st}}} + v_{i_{\text{imp}}} + v_{i_{\text{bund}}}}. \tag{2}$$

The corresponding volume fraction of each material (v and the corresponding subscripts) can be calculated with the packing factor (PF), usually provided by the manufacturer. Furthermore, an additional term is added to consider the conductivity of the external cover insulator of the bundle, designated by the subscript bund. This modification of the Hashin–Shtrikman's approach shows an error in the estimation of k_w compared with measurements lower than 11% for low PF litz bundles (PF $< 50\%$) and lower than 37% for high PF bundles (PF $> 50\%$), according to [15].

For higher PF (PF $> 50\%$), other methods have been recently presented. In [16], a thermo-electric field analogy to estimate the effective k_w of litz bundles is developed. A deviation from measurements between 1.3% and 12.5% is achieved with this approach, but it is a relatively complex method. The methodology from [17] and [18] is based in thermal networks. Both use the available data from the manufacturer and provide good matching with FEA results. The first one provides different models for square-packed and hexagonal-packed wires, but does not offer

experimental data. The second one provides experimental results with good accuracy. However, it requires some experimental calibration, since there is a strong dependence on the uncertainty associated to manufacturing tolerances and material data provided by the litz manufacturers. By analyzing the results from [18], it can be stated that this error margin is lower than 34%. Therefore, using the modified Hashin–Shtrikman's method from [15] leads to results close or within that uncertainty band.

To summarize, Hashin–Shtrikman's method with the averaged properties of the insulation materials offers proper accuracy for low PF values. For higher values, other methods such as the ones provided in [17] and [18] are recommended, but require additional complexity or calibration with measurements due to the manufacturing uncertainty. In that case, modified Hashin–Shtrikman's method (1) and (2) can be used for simplicity, since its accuracy is acceptable. As described in Section IV, this approach offers a good matching with experimental results.

B. Winding-Level Homogenization

Once the homogeneous conductivity of a wire k_w is obtained, the next step is to characterize the effective thermal conductivity of the whole winding of the magnetic component k_{eq}. This comprises every homogenized wire (k_w) and the surrounding material between them (see Fig. 2).

This second homogenization implies the geometric transformation of every homogenized wire to a single block. As a result, the external heat exchange surface with the air is slightly modified, as well as the contact resistance between the equivalent winding and the core. However, this effect has been neglected, since its contribution have a minimum effect on the global heat transfer.

It is important to highlight that uniform power distribution is assumed. The power losses generated in the original system remain unchanged in the equivalent model. As an example, to analyze an inductor with 100 wires and 2 W total winding losses, the 2 W will be assigned to the equivalent block.

The guidelines to model round wires (solid and litz), square litz wire, and foil for inductors are described along the following sections.

1) Round Wires (Solid and Litz): The analytical homogenization techniques summarized in [10] could be use to calculate k_{eq} for round wires (solid or litz). However, their accuracy is limited for low filling ratios, which is common in composite materials for which they were developed. On the other hand, the wires in a magnetic component are usually arranged very close to each other, leading to high filling ratios within the window. Then, those approaches are not recommended and a more accurate model is required.

A new generalized model based on a multivariable curve fitting of FEA simulation results is introduced in this paper in order to increase the accuracy and avoid the previous limitation. The simulation setup is depicted in Fig. 3, similar to the process to obtain the effective thermal conductivity described in [7] and [8]. The depicted "cell" is a representative cross-sectional sample of the winding, as shown in Fig. 2. This cell contains a wire (with conductivity k_w) and the surrounding material (i.e., potting resin or air, with conductivity k_a). The diameter of the wire is ϕ and the width of the representative cell is w. Since this cell is "repeated" along the window of the magnetic component, the top and bottom surfaces are defined as adiabatic, to account for this symmetry [7]. Then, since the goal of this analysis is to obtain the effective thermal conductivity across the cell, certain heat flux q''_x [W/m^2] is injected on the left surface of the cell. As a consequence, a temperature gradient appears between the left and the right surfaces, considering T_1 and T_2 as the average surface temperatures in [K] on left and right surfaces, respectively. Hence, the effective thermal conductivity k_{eq} between left and right surfaces is calculated as the product of the applied heat flux (q''_x) and the width of the cell (w) divided by the temperature rise between surfaces ($\Delta T = T_1 - T_2$) according to

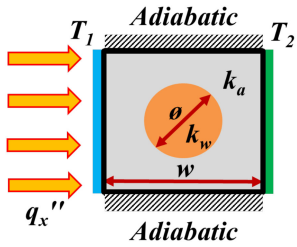

Fig. 3. Cross-sectional representation of the simulation setup.

$$k_{\text{eq}} = q''_x \cdot \frac{w}{\Delta T} = q''_x \cdot \frac{w}{T_1 - T_2}. \tag{3}$$

The effective thermal conductivity of the winding k_{eq} depends on the ratio between the thermal conductivity of the wire and the surrounding material $k_{\text{ratio}} = k_w/k_a$, and their volume fractions, which can be expressed in terms of the relationship between the diameter of the wire over the width of the cell ϕ/w. Obtaining this relationship by analytical methods becomes quite complex, therefore 2-D FEA simulations are used instead (according to the setup shown in Fig. 3). In order to get the effective conductivity for any combination of size and conductivity ratios, a high enough number of simulations are solved. In this case, a sweep of 31 steps from 0.5 and 0.8, and 100 more from 0.8 to 0.998 for ϕ/w are considered. On the other hand, k_{ratio} is swept with 600 logarithmic steps from 10^0 to 10^5. For each combination of k_{ratio} and ϕ/w, the effective thermal conductivity k_{eq} is obtained by simulation. These results are shown in Fig. 4.

Then, a multivariable fitting of the resultant graph was performed to get a general expression for k_{eq} applicable to any k_{ratio} from 1 to 100 000 and ϕ/w from 0.5 to 1—for lower size ratios, any of the traditional methods can be used, since they offer a negligible error. To do so, (4) is proposed. It consists of a modification of Hashin–Shtrikman's equation, where the volume fraction τ is replaced by a variable τ^*, described as

$$\frac{k_{\text{eq}}}{k_a} = \frac{(1+\tau^*)\cdot k_{\text{ratio}} + (1-\tau^*)}{(1-\tau^*)\cdot k_{\text{ratio}} + (1+\tau^*)} \tag{4}$$

where τ^* is a variable obtained such that its value makes the above-mentioned equation to get the exact value of k_{eq} from the

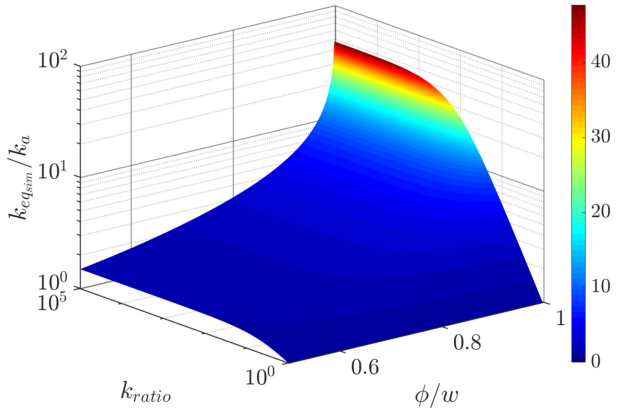

Fig. 4. Effective thermal conductivity of a cell: simulation results of k_{eq}/k_a over k_{ratio} and ϕ/w.

simulations. It is expressed as

$$\tau^* = \frac{\pi}{4} \cdot \left(\frac{\phi}{w}\right)^2 + a \cdot \left(\frac{\phi}{w}\right)^b + c \cdot \left(\frac{\phi}{w}\right)^d. \tag{5}$$

Whose coefficients a, b, c, and d are expressed in terms of k_{ratio} according to (6). Notice that coefficients c and d are 0 for k_{ratio} lower than 6.7; their values depend on k_{ratio} calculated as

$$a = \frac{0.15323 \cdot k_{\text{ratio}} - 0.21445}{k_{\text{ratio}} + 6.1801} \tag{6a}$$

$$b = \frac{14.297 \cdot k_{\text{ratio}} + 78.569}{k_{\text{ratio}} + 8.3734} \tag{6b}$$

$$c = \begin{cases} 0 & k_{\text{ratio}} < 6.7 \\ \dfrac{0.04902 \cdot k_{\text{ratio}} - 0.24267}{k_{\text{ratio}} + 19.568} & 6.7 \leq k_{\text{ratio}} \end{cases} \tag{6c}$$

$$d = \begin{cases} 0 & k_{\text{ratio}} < 6.7 \\ \dfrac{270.55 \cdot k_{\text{ratio}} - 472.41}{k_{\text{ratio}} + 3.6959} & 6.7 \leq k_{\text{ratio}}. \end{cases} \tag{6d}$$

The results obtained by the above-mentioned equations are compared to the aforementioned approaches from [10] (Hashin–Shtrikman, Maxwell, Rayleigh, and Milton) and FEA results. To make this comparison, the relative error ($\text{Error}[\%] = (k_{\text{estimated}}/k_{\text{simulated}} - 1) \cdot 100$) for those approaches is plotted over ϕ/w and k_{ratio} in Fig. 5. It can be seen that Hashin–Shtrikman, Maxwell, and Rayleigh methods might result in an underestimation of k_{eq} of 83%, 95%, and 88%, respectively. The mismatch of Milton's approach varies from $+18\%$ to -75%. This could lead to unacceptable estimations of the temperature rise. However, the proposed method shows a better performance, with a little error in the band of $[-2.4, 4.6]\%$. This fact reveals that the developed method shown in this paper is more suitable for the homogenization of round conductors than other traditional approaches.

2) Square Litz Wires: Since square litz wires lead to high filling factor of the magnetic component's window, the space between the bundles is negligible. Then, only the first step of the homogenization is required. The procedure to obtain an equivalent thermal conductivity in this case corresponds to the one described in Section II-A2. The equivalent conductivity of the winding will be equal to the obtained k_w in that section.

3) Foil: Foil is a useful choice for high-frequency specifications [19] and provides a lower thermal impedance path than litz or solid wires, since the heat exchange surface between layers is much higher. The homogenized thermal conductivity of a foil winding can be easily obtained if there is no insulation. In that case, the equivalent conductivity of the winding can be approximated to the conductor's conductivity, neglecting the air between the layers. However, if some insulation layer exists between the conductor layers, the effective thermal conductivity requires some further calculations, depending on the shape of the winding (rectangular or circular). To analyze these problems, 1-D heat transfer equation can be solved to get effective thermal conductivity of the winding for each spatial direction, as described next.

XY rectangular winding: If the center core leg is squared and the conductor and the insulation layers are alternated, a simple thermal network in Cartesian coordinates can be analyzed to extract the effective conductivity for each spatial direction: orthogonal direction ($k_{\text{eq}_{\text{ort}}}$) across the perpendicular direction to the winding; top-down direction (k_{eq_z}) along the vertical direction of the winding; tangential direction ($k_{\text{eq}_{\text{tan}}}$) along the winding direction.

Solving the corresponding 1-D thermal networks corresponding to Fig. 6 (see Appendix A for further details), the thermal conductivity in the orthogonal directions is defined as

$$\frac{1}{k_{\text{eq}_{\text{ort}}}} = \frac{1}{k_{\text{cond}}} \cdot \frac{l_{\text{cond}}}{l_{\text{cond}} + l_{\text{ins}}} + \frac{1}{k_{\text{ins}}} \cdot \frac{l_{\text{ins}}}{l_{\text{cond}} + l_{\text{ins}}} \tag{7}$$

where l_{cond} and l_{ins} are the total width of conductor and insulation layers, respectively. As an example, in Fig. 6, considering the red layers as conductors and yellow ones as insulation, $l_{\text{cond}} = l_1 + l_3$ and $l_{\text{ins}} = l_2 + l_4$); k_{cond} and k_{ins} are their corresponding conductivity.

Regarding the vertical direction, the conductivity can be expressed as

$$k_{\text{eq}_z} = k_{\text{cond}} \cdot \frac{A_{\text{cond}}}{A_{\text{cond}} + A_{\text{ins}}} + k_{\text{ins}} \cdot \frac{A_{\text{ins}}}{A_{\text{cond}} + A_{\text{ins}}} \tag{8}$$

where A_{cond} and A_{ins} are total heat exchange cross sections of both the conductor and the insulation tape ($A_{\text{cond}} = A_1 + A_3$ and $A_{\text{ins}} = A_2 + A_4$).

Finally, the impact of the tangential conductivity on the heat flow along this direction can be ignored, since the temperature gradient along the same foil layer is negligible because the winding is a heat source itself and it has axial symmetry. Thus, the problem is similar to a composite plane wall.

RZ Circular winding: In a similar manner, a 1-D thermal network is analyzed in cylindrical coordinates to get an equivalent conductivity when a round center core leg is studied. This case is shown in Fig. 7 (see Appendix A for further details). The radial component of the equivalent conductivity is expressed as

$$k_{\text{eq}_r} = \frac{ln(\frac{r_n}{r_1}) \cdot k_{\text{cond}} \cdot k_{\text{ins}}}{k_{\text{ins}} \sum_{n_{\text{cond}}} ln(\frac{r_{n+1}}{r_n}) + k_{\text{cond}} \sum_{n_{\text{ins}}} ln(\frac{r_{n+1}}{r_n})} \tag{9}$$

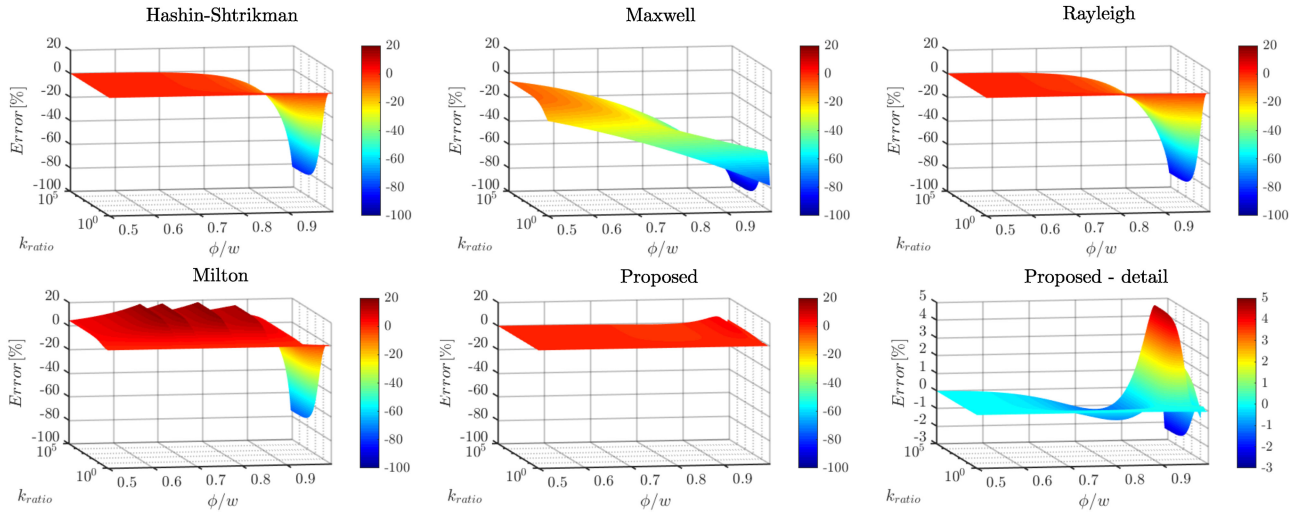

Fig. 5. Relative error in the estimation of the effective thermal conductivity calculated with traditional approaches and the proposed method.

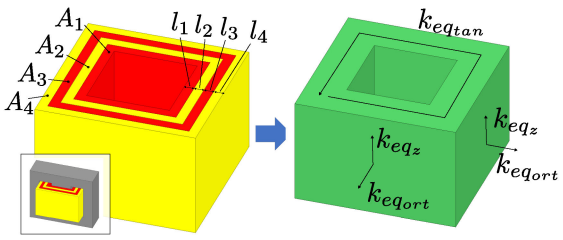

Fig. 6. Foil winding for squared cores (left) and equivalent winding (right).

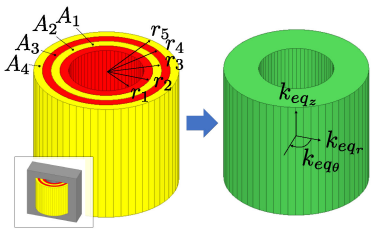

Fig. 7. Foil winding for round cores (left) and equivalent winding (right).

where n_{cond} refers to the conductor layers and n_{ins} to the insulation layers (in the example in Fig. 7: $n_{\text{cond}} = 1, 3$ and $n_{\text{ins}} = 2, 4$).

The conductivity along the vertical direction is described in (8). Finally, the impact of the conductivity along the θ direction can be ignored, due to the same reasoning that $k_{\text{eq}_{\text{tan}}}$ previously described.

C. Summary

Finally, the two-level homogenization process is summarized in Table I for the different winding types, to ease the readability. In any case, additional design steps from Section III will be followed if interleaving or insulation are used.

III. Use of the Two-Level Homogenization for Transformers

So far, the procedure to homogenize a magnetic component made by a single winding type has been explained. That is the typical case of an inductor. However, if different wires (size or type) are used in the same component, some further steps need to be carried out. A clear example of this is a transformer, in which the diameter of the wires from primary and secondary is different.

Some considerations to apply the introduced method to transformers, where interleaving techniques and insulation tape might be used, are described in this section.

A. Application to Different Interleaving Levels

The different levels of interleaving are depicted in Fig. 8 and described next.

1) Winding arrangement in blocks. Primary and secondary windings are separately treated since the diameter of their wires could be different, as well as their losses. Then, the corresponding effective thermal conductivity for each winding k_{eq_1} and k_{eq_2} is calculated according to Section II.
2) Layer-level interleaving. The procedure to compute k_{eq_1} and k_{eq_2} do not differ from the previous case, but the corresponding equivalent blocks are alternated according to the primary and secondary arrangement.
3) Fully interleaved winding. Since primary and secondary wires are alternated within the same layer, the only solution is to homogenize the whole winding as one single block. First, the effective thermal conductivity of each cell is calculated (k_{eq1} and k_{eq2}). Then, (8) is used to obtain the effective conductivity of each layer. Finally, depending on the shape of the center leg of the magnetic component, the corresponding equations from Section II-B3 will be used to get the total effective conductivity $k_{\text{eq}_{\text{TOT}}}$.

TABLE I
EQUATIONS SUMMARY FOR DIFFERENT WINDING TYPES

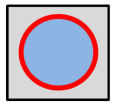	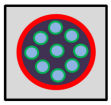	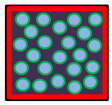	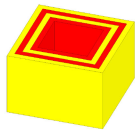	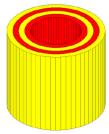
Round solid wire	**Round litz bundle**	**Square litz bundle**	**Square foil**	**Round foil**
1) $k_w = k_{cond}$.	1) k_w (Eq. 1 and 2).	1) $k_{eq} = k_w$ (Eq. 1 and 2).	1) $k_{eq_{ort}}$ (Eq. 7).	1) k_{eq_r} (Eq. 9).
2) k_{eq} (Eq. 4-6).	2) k_{eq} (Eq. 4-6).		2) k_{eq_z} (Eq. 8).	2) k_{eq_z} (Eq. 8).

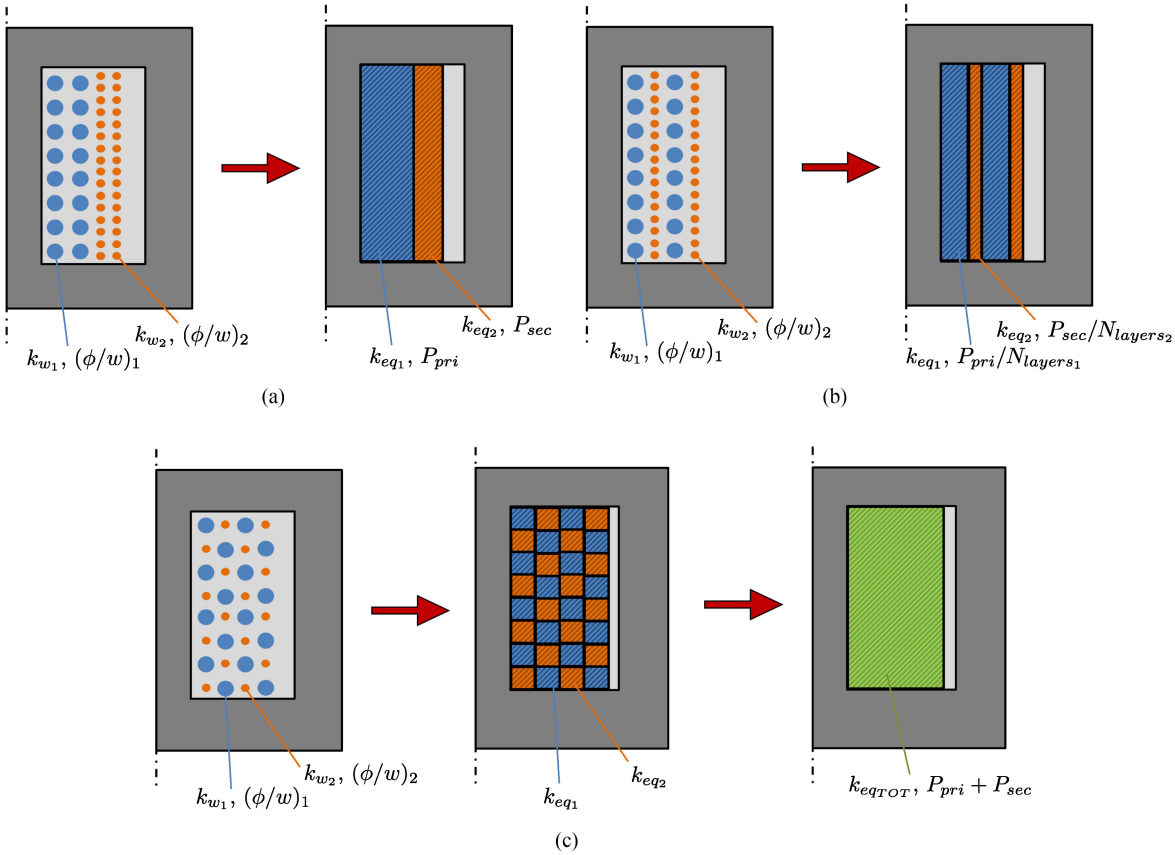

Fig. 8. Homogenization procedure for different winding arrangements in transformers. (a) Winding arrangement in blocks. (b) Layer-level interleaving. (c) Fully interleaved winding.

1) Losses Assignation: It is important to notice that an EM homogenization is required prior to perform the thermal simulation to consider the non-uniform losses distribution due to high-frequency effects. Some EM homogenization techniques are proposed in [20]–[23]. By using these approaches, both the EM and thermal simulations can be coupled in the simulation software. Further details are provided in Section IV-B.

In the case that the EM-thermal coupling was not an available feature of the used simulation tool, certain simplifications could be performed depending on the interleaving level. For a winding arrangement in blocks [see Fig. 8(a)], the total primary losses P_{pri} and total secondary losses P_{sec} would be assigned to the blocks k_{eq_1} and k_{eq_2}, respectively (see Fig. 8). For a layer-level interleaving, the assigned losses to each equivalent layer would correspond to the proportional part of the number of layers (N_{layers_1} and N_{layers_2}). For example, if primary winding dissipates 1 W and there are five layers, the losses will be equally split among them (1 W$/5 = 0.2$ W per primary layer). Finally, in a fully interleaved winding, since both primary and secondary windings are homogenized as a single block, the assigned losses to this block would be equal to the total winding losses. However, using these simplifications would penalize the accuracy of the obtained temperature compared to the EM-thermal coupling. Then, it is recommended to use EM-thermal coupling if possible.

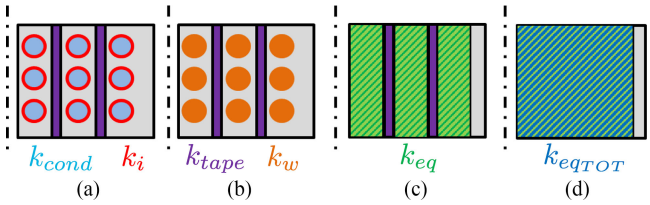

Fig. 9. Representation of a winding modeling with insulation tape. (a) Original winding. (b) First homogenization. (c) Second homogenization. (d) Tape and winding layers homogenization.

B. Insulation Tape Between Layers

It is a common practice to add some insulation tape, usually between primary and secondary winding in a transformer. As an example, the process to model this case is depicted in Fig. 9. The first step [from Fig. 9(a) to (b)] is to homogenize each conductor, according to Section II-A (wire-level homogenization), obtaining their k_w. Next, each layer separated between tape layers is homogenized, following the procedure from Section II-B (winding-level homogenization), assigning to them their corresponding k_{eq} [see Fig. 9(c)]. Optionally, every insulation tape and winding layer can be homogenized in a single block with conductivity $k_{\text{eq}_{\text{TOT}}}$, by treating them as foil layers, using the corresponding equations from Section II-B3 [see Fig. 9(d)].

At this point, the procedure to obtain a simplified thermal model for any inductor or transformer with round, square, or foil winding, also with interleaving or insulation if needed, is explained. The method is validated by means of experimental results in the following Section.

IV. Experimental Validation of the Model

In this section, the scope of the suggested homogenization technique is analyzed and validated in two different scenarios: DC and AC excitation currents. The corresponding testbench is depicted in Fig. 10. In (a), the device under test is connected to a voltage source at constant voltage, so a DC current is injected to the magnetic component. In (b), a sinusoid is provided by a waveform generator (GW Instek, model AFG-2005), which is amplified by an RF amplifier (AR, model 150A 100B) and then connected to the magnetic component in order to analyze the high-frequency effects of an AC current. In the case of an inductor (b.1), it is connected in series to a capacitor. The impedance of this resonant series *LC* tank is minimum at its resonant frequency, with the purpose of injecting a high peak current with an acceptable voltage level at that frequency. In the case of a transformer (b.2), a resistive load of 1 Ω is connected in its secondary side in order to have AC current flowing through both primary and secondary windings.

As a result of injecting either DC or AC current, some EM losses are caused in the tested magnetic component. Then, its temperature starts rising until the thermal steady state is reached. The goal of this testbench is obtaining experimental measurements of this temperature rise and comparing it with a detailed

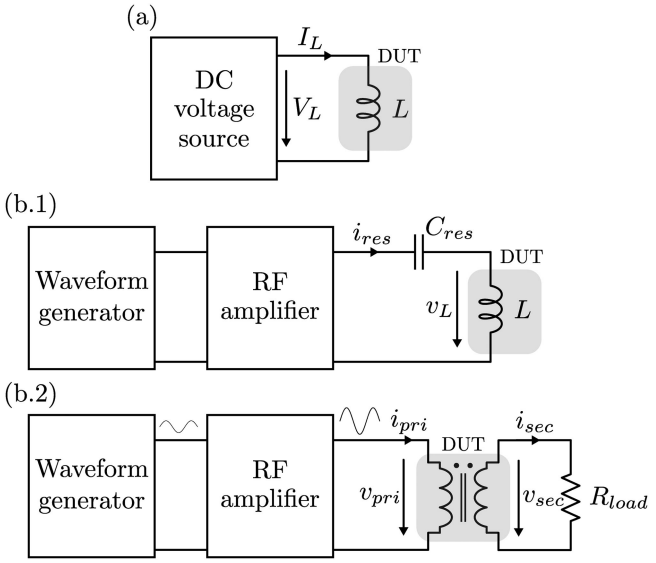

Fig. 10. Testbench for (a) DC excitation in inductors, and AC excitation in (b.1) inductors and (b.2) transformers.

3-D FEA simulation ("wire-level FEA") and other 3-D FEA simulation using the method developed in this paper ("winding-level FEA"). The differences between both simulations are described next.

1) "Wire-level FEA." Fully detailed 3-D FEA simulations, which include the insulation of the wires or the strands within a litz bundle, are not feasible due to the highly demanding meshing of these objects [21]. As a result, at least the wire-level homogenization described in Section II-A is mandatory and applied in these "wire-level FEA" 3-D simulations.
2) "Winding-level FEA." In this case, the suggested two-step homogenization is used, every wire from the previous step and the material between them are homogenized, according to Sections II-B and III. This two-step homogenization leads to a considerably reduced simulation time compared with the "wire-level FEA" approach, which will be analyzed at the end of this section.

To compare both 3-D simulations with the experimental results, mean surface temperatures of the core, and the winding of each magnetic component are measured with a FLUKE-Ti400 thermal camera, according to the procedure described in [24]–[26]. The 3-D simulations are performed with Icepak, from ANSYS Electronics Desktop 2019.1.

Several inductors and a transformer, with different core shapes and winding types, are tested to validate the introduced homogenization method under different scenarios, described in Table II. The next thermal conductivity has been considered for the different objects or materials in all cases: $k_{\text{fe}} = 4.5$ W/m· K for the ferrite cores [27], $k_a = k_{\text{imp}} = 0.03$ W/m· K (conductivity of air at 353 K from [28]) for the air surrounding the wires and the "impregnation material" of the litz bundles, $k_{i_{\text{bund}}} = 0.155$ and $k_{i_{\text{st}}} = 0.245$ W/m· K [16] for the bundle insulation and strand

TABLE II
DESCRIPTION OF THE TESTED PROTOTYPES

Prototype	A (inductor)	B (inductor)	C (inductor)	D (inductor)	E (transformer)
Core	P36/22	P36/22	PQ32/30	PQ32/30	RM8/I
Winding type	Solid	Litz 35 x 0.2mm	Litz 35 x 0.2mm	Foil (0.27mm·2) (cop.+iso.+cop.+iso.)	Solid
ϕ[mm]	0.81 (AWG20)	1.45 (AWG15)	1.45 (AWG15)	—	pri=0.51 (AWG24), sec=0.81 (AWG20)
insulation thickness[mm]	0.02	0.055	0.055	65μm (·2)	0.02
w[mm]	0.87	1.6	1.6	4	pri=0.64, sec=1
Number of turns	92	28	42	22	pri=28, sec=15
k_w[W/mK]	390	0.205309	0.205309	390	390
k_{eq}[W/mK]	0.179535	0.079864	0.079864	1.4094	pri=0.0639, sec=0.0721

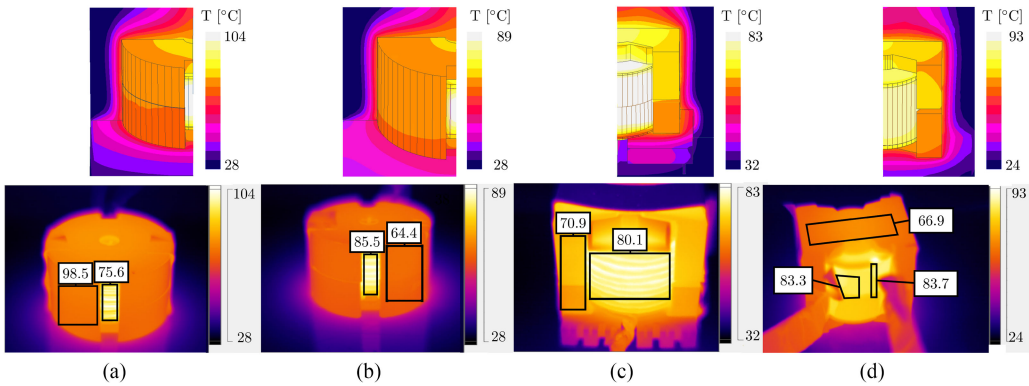

Fig. 11. DC test thermal results: on the upper row, results of the "winding-level FEA" 3-D thermal simulations of the prototypes A, B, C, and D from left to right; on the bottom row, the corresponding experimental thermography including the averaged temperature in the marked black squares.

insulation materials. The accuracy and simulation speed results are analyzed along the following sections.

The results presented for each prototype are calculated in 3-D simulations and extracted from the thermography (FLUKE Smart View software). The measurements from the thermal camera are considered as the reference for the surface temperatures. Then, the relative error between the measured temperature rise ($\Delta T_{\text{exp}} = T_{\text{exp}} - T_{\text{amb}}$) and the temperature rise obtained by the corresponding 3-D simulation ($\Delta T_{\text{sim}} = T_{\text{sim}} - T_{\text{amb}}$) is calculated according to

$$\text{Error}_{T\text{surf}}[\%] = \left(\frac{\Delta T_{\text{sim}}}{\Delta T_{\text{exp}}} - 1\right) \cdot 100. \tag{10}$$

Regarding the maximum temperature estimation, since measuring the temperature within the core is not possible, only the results from "wire-level FEA" (just wires/bundles are homogenized) and "winding-level FEA" (two-stage homogenization is performed) 3-D simulations are compared. In this comparison, the "wire-level FEA" is considered as the reference, so the relative error of these magnitudes is calculated with

$$\text{Error}_{T\max}[\%] = \left(\frac{\Delta T_{\text{windFEA}}}{\Delta T_{\text{wireFEA}}} - 1\right) \cdot 100. \tag{11}$$

TABLE III
DC TEST CONDITIONS

Prototype	A	B	C	D
T_{amb}[°C]	26	24	26	20
P[W]	3.793	3.244	3.160	4

A. DC Tests

In this section, some DC current is injected into the inductors "A," "B," "C," and "D" in order to have certain winding conduction losses while having null core loss, according to the setup depicted in Fig. 10. Power loss and ambient temperature for each test are summarized in Table III. The temperature distribution obtained with the thermal camera and the suggested 3-D "winding-level FEA" simulations corresponding to this tests is

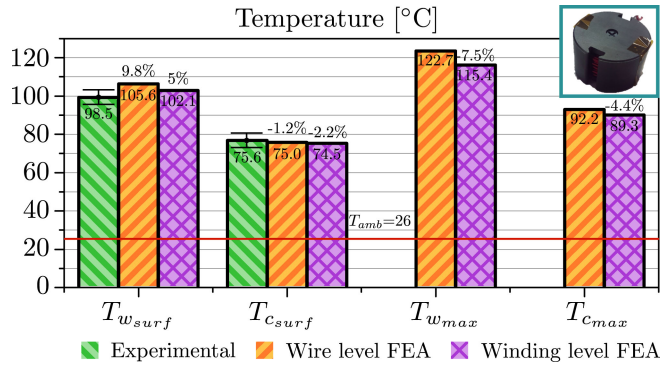

Fig. 12. DC test temperature of "A" (P36/22 inductor, round solid wire).

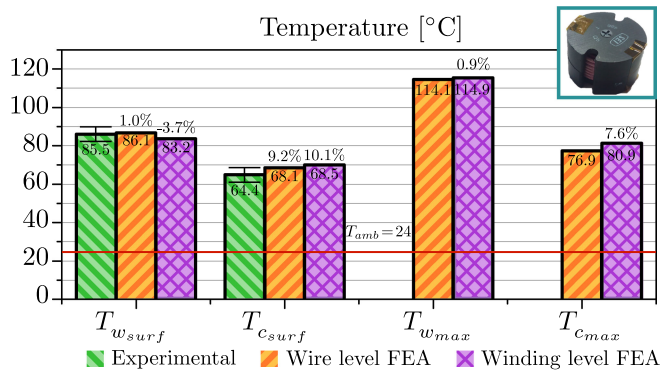

Fig. 13. DC test temperature of "B" (P36/22 inductor, round litz bundle).

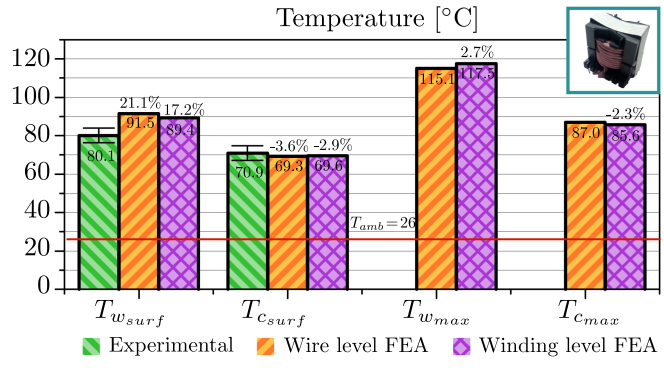

Fig. 14. DC test temperature of "C" (PQ32/20 inductor, round litz bundle).

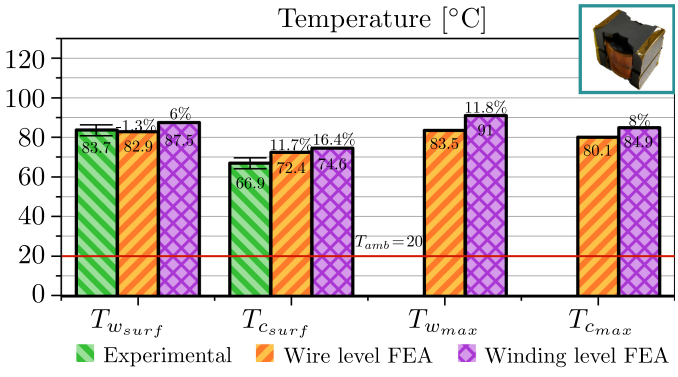

Fig. 15. DC test temperature of "D" (PQ32/20 inductor, foil).

shown in Fig. 11. Mean and maximum temperatures in the core and the winding of each device are analyzed next to validate the proposed model for DC excitation.

For each prototype, the results are presented in bar graphs. The bars, respectively, correspond to the experimental, "wire-level FEA" and "winding-level FEA" obtained temperatures (bars for experimental maximum temperatures are not shown since that data are not available). The error margin inherent to the measurements, which is related to the discrepancy of the measured surface emissivity and the background radiation, is included for every case.

1) Prototype A. Inductor, P36/22, Round Solid Copper: As a proof of concept of the homogenization at the winding level (see Section II-B), a pot core inductor with round solid wire is built. Since the winding is practically surrounded by the core, the external boundary conditions practically do not affect it, thus avoiding a possible source of error. The results of this test are shown in Fig. 12. It can be seen that the simulation with the equivalent layer ("winding-level FEA") deviates only a 5% for the winding surface temperature estimation ($T_{w_{\text{surf}}}$) and -2.2% for the core surface temperature ($T_{c_{\text{surf}}}$). Furthermore, the evaluation of the maximum temperatures in winding ($T_{w_{\text{max}}}$) and core ($T_{c_{\text{max}}}$), respectively, have -7.5% and -4.4% deviation, compared with the detailed "wire-level FEA" simulation.

2) Prototype B. Inductor, P36/22, Round Litz: Prototype B consists in an inductor, with the same core than the previous one, but with round litz wire. In this case, the performance of both wire-level (see Section II-A) together with the winding-level homogenization (see Section II-B) can be checked. The data of the litz wire provided by the manufacturers has certain tolerance, so there is some uncertainty. However, the results of the "winding-level FEA" simulation are close to the "wire-level FEA" estimations, as depicted in Fig. 13. The evalution of $T_{w_{\text{surf}}}$ has almost no deviation compared with the experimental measurement (1% and -3.7%, respectively) and a slightly higher for $T_{c_{\text{surf}}}$ (9.2% and 10.1%). This might be due to a mismatch of the boundary conditions in the simulations with respect to the experimental setup.

Comparing prototypes A and B, they both use a P36/22 core, but A is made by solid wires and B by litz bundles. After the winding homogenization, the wires are replaced by a block. This change in the geometry leads to a different external surface exposed to the ambient (lower external surface after the homogenization). Since the solid wires from A are more compactly packed than B, the decrement of external surface is lower in A than in B. Consequently, the impact of convective heat transfer is stronger in A than in B after the winding homogenization. This is the reason why the maximum winding temperature after the homogenization is higher after the winding homogenization (two-level homogenization) in A and lower in B, compared with their corresponding wire homogenization (first-level homogenization).

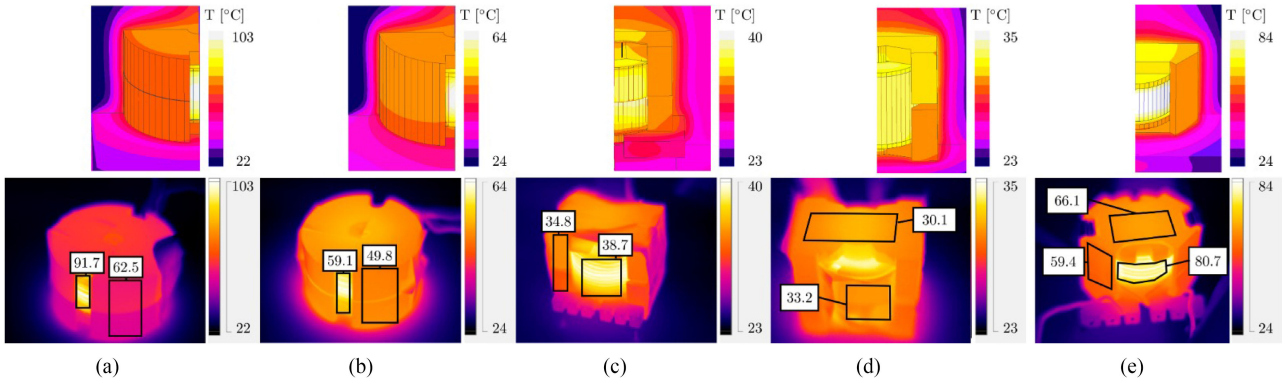

Fig. 16. AC test thermal results: on the upper row, results of the "winding-level FEA" 3-D thermal simulations of the prototypes A, B, C, D, and E from left to right; on the bottom row, the corresponding experimental thermography including the averaged temperature in the marked black squares.

TABLE IV
AC TEST CONDITIONS

Prototype	**A**	B	C	D	E
T_{amb}[°C]	24	22	23	22	20
f[kHz]	62	219	155	107	100
I_{pk-pk}[A]	3.2	3.49	4.74	3.68	$pri = 3.68$ $sec = 6.64$

However, the important point here is that the "winding-level FEA" simulation offers close results to the "wire-level FEA," but with a much less demanding mesh and, thus, a lower simulation time, which will be analyzed at the end of this section.

3) Prototype C. Inductor, PQ32/20, Round Litz: Once the performance of the two-step homogenization is checked, a PQ core inductor is built to check the performance of the equivalent layer when it is in direct contact with the ambient. Due to the addition of this condition, another uncertainty appears, as previously explained. This is the reason of a higher deviation of $T_{w_{\text{surf}}}$ (see Fig. 14). But still, the highlight of this comparison is the similarity of the results of both simulations, so the "winding-level FEA" simulation offer the additional advantage of having a much simpler mesh.

4) Prototype D. Inductor, PQ32/20, Foil: Another concept presented in this paper is the homogenization of foil wound magnetic components. To validate the expressions from Section II-B3, a PQ core inductor with foil winding is built. As shown in Fig. 15, the estimation of $T_{w_{\text{surf}}}$ and $T_{c_{\text{surf}}}$ has an acceptable deviation from the measurements. Comparing this case with the previous ones, the evaluation of the maximum temperatures are slightly higher with the "winding-level FEA" model.

B. AC Tests

Along this section, AC excitation is used instead of DC in every inductor (prototypes "A," "B," "C," and "D"). A transformer is added (prototype "E"), where proximity effect becomes more critical. In AC excitation, some local effects within the wires appear (skin and proximity effects), but the resultant loss distribution can be directly mapped in the thermal simulation [29]. The AC setup is depicted in Fig. 10. The peak-to-peak of the sinusoidal current and frequency for each case (equal to the resonant frequency of the *LC* tank), as well as the ambient temperature, are summarized in Table IV. The temperature maps obtained in simulation and by measurements are shown in Fig. 16.

Prior to the 3-D thermal simulations, a 3-D EM simulation corresponding to the electrical operating conditions is required to obtain the power loss distribution in every finite element. This power loss distribution is directly mapped into the 3-D thermal simulation as an input [29]. In this way, the high-frequency effect on the losses distribution is considered.

Furthermore, the EM equivalent properties need to be calculated and assigned in the "winding-level FEA" simulations. To calculate these EM properties, some homogenization techniques are proposed in [20]–[23]. For the sake of simplicity, [20] is used in the corresponding EM simulations required in this section. In the AC tests shown next, two new variables are added, compared to the DC tests, which could be sources of deviation between measurements and simulations: core loss and the EM homogenization. The results for each prototype are described next.

1) Prototype A. Inductor, P36/22, Round Solid Copper: In this test, the difference with measured mean temperatures of winding and core is higher than in the previous DC case. The main reason of this is the uncertainty related to the assigned EM material properties and the EM homogenization. However, it can be seen in Fig. 17 that both "wire-level FEA" and "winding-level FEA" have close results.

2) Prototype B. Inductor, P36/22, Round Litz: The temperature rise in prototype B is lower than in prototype A for a current of similar magnitude (see Table IV) due to the lower resistance of used litz bundle compared to the round solid wire (Fig. 18). Simulation results are within the measurement error margin and close to each other (differences of 2.5% and 1.2% for maximum temperatures).

3) Prototype C. Inductor, PQ32/20, Round Litz: By means of prototype C, the validation is carried out for a litz-based winding in a highly exposed to ambient core shape with AC excitation (Fig. 19). In this case, the maximum possible current (due to hardware limitations) is set, according to Table IV. Even with

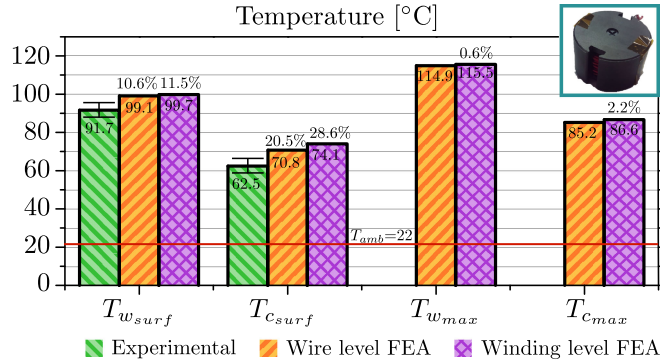

Fig. 17. AC test temperature of "A" (P36/22 inductor, round solid wire).

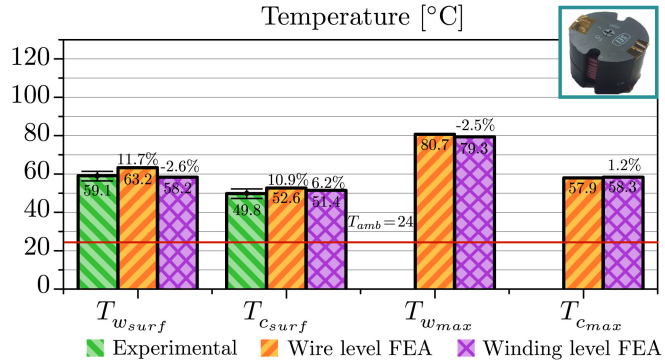

Fig. 18. AC test temperature of "B" (P36/22 inductor, round litz bundle).

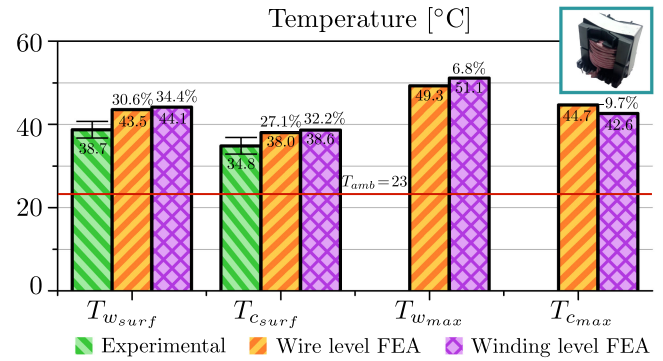

Fig. 19. AC test temperature of "C" (PQ32/20 inductor, round litz bundle).

this current, the temperature rise is lower than the previous cases due to the reduced resistance of this winding. As a consequence, the relative error between measurements and errors is higher. However, in terms of absolute error, the difference is around 5° C.

4) Prototype D. Inductor, PQ32/20, Foil: The homogenization of foil winding, described in Section II-B3, is validated with AC current (Fig. 20). Nevertheless, the same conclusion can be extracted than in Prototype D, except that the deviation of the simulation results is within the measurement error margin.

5) Prototype E. Transformer, RM8/I, Round Solid Wire: The last concept that needs to be validated is the homogenization applied to transformers. To do so, an RM8/I core transformer with solid copper wires of different diameters for primary and

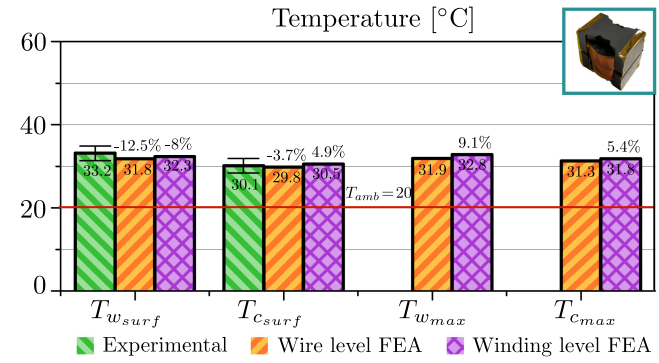

Fig. 20. AC test temperature of "D" (PQ32/20 inductor, foil).

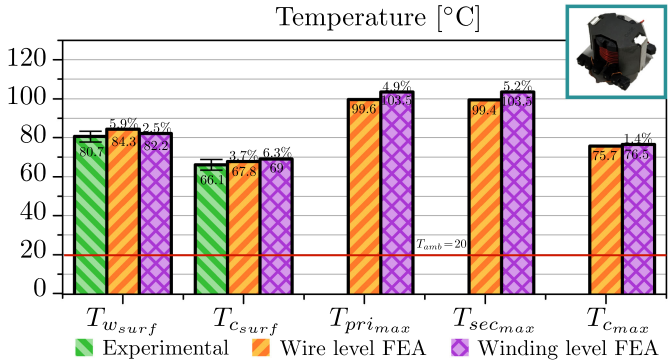

Fig. 21. AC test temperature of "E" (RM8/I transformer, round solid wire).

secondary windings is tested, according to Fig. 10 and Table IV. The results are shown in Fig. 21. It can be seen that the deviation between simulations and measurements is lower than 6.3%. Furthermore, the results of both "wire-level FEA" and "winding-level FEA" differ in less than 5.2%.

C. DC and AC Results Summary

Regarding the previous results of the DC and AC tests, the next general conclusions can be extracted.

1) Thermal measurements have an inherent error due to the discrepancy in the emissivity of the measured surfaces and the background radiation [24]–[26].
2) Difference between the 3-D thermal simulations using both the "wire-level FEA" approach or the proposed "winding-level FEA" and measurements is affected by the tolerance of the available thermal and EM material properties data provided by the manufacturers.
3) In the case of the AC tests, two additional variables appear: core loss and the EM homogenization required for the "winding-level FEA."
4) Due to the geometric modification in the "winding-level FEA" approach, the impact of the convective heat transfer is slightly varied compared with the detailed "wire-level FEA." However, the difference between each other is lower than 5° C for most cases, except for the foil inductor, where it is lower than 9° C.

TABLE V
COMPUTATION TIME FOR PROTOTYPES A, B, C, D, AND E WITH THE WIRE-LEVEL FEA AND THE EQUIVALENT LAYER

Prototype	A	B	C	D	E
Wire level FEA	20'29"	19'25"	20'17"	10'55"	25'46"
Winding level FEA	2'55"	3'08"	2'48"	1'32"	3'11"
Reduction factor	7	6.2	7.2	7.1	8.1

The most remarkable key point is the accuracy of the introduced two-stage thermal homogenization ("winding-level FEA") in addition to its reduced simulation time, compared with detailed simulations ("wire-level FEA"), which is analyzed next.

D. Finite Element Simulations: Computation Time

Once the accuracy of the method is analyzed, the simulation time saving due to the simpler mesh of the "winding-level FEA" simulation is compared with the detailed "wire-level FEA" simulation for each prototype in Table V. It is remarkable that the "winding-level FEA" leads to a reduction of the computation time by a factor between 6 and 8.

The results are computed with the Icepak pacakge from ANSYS Electronics Desktop 19.1, running Intel Core i7-6700 CPU and 32 GB RAM is used. The mesh level is set as default and 100 iterations with the solve setting set to "Flow = 0.0001" and Energy to "1e-8."

To summarize, the proposed method is validated by the previous experimental results. Furthermore, it provides almost the same performance than detailed simulations—in terms of accuracy—in addition to a much simpler mesh, which leads a considerable reduction of the required simulation time.

V. CONCLUSION

A two-step homogenization is introduced in this paper to simplify the thermal analysis of the magnetic components used in power electronics, while keeping high accuracy. The required analytical equations and specific guidelines to model round solid and litz wires, square litz wire, and foil wound magnetics are described. Other special concerns are discussed, such as the modeling of transformers with interleaving and the use of insulation tape between layers.

The main advantage of this method is that it reduces the required time for 3-D thermal simulations by a factor of 6–8, while keeping almost the same accuracy than more detailed simulations. Experimental prototypes (four inductors and one transformer) are built to validate this method, both with DC and AC excitation. Other contribution of this method is that convergence of 3-D simulations is assured even for complex structures or litz winding, since the required mesh is much less demanding for the equivalent winding than for detailed simulations. These improvements might allow using this equivalent 3-D thermal simulations within optimization processes and sensitivity analysis, thus providing more accurate temperature estimations than traditional analytical equations, leading to higher power density magnetic components.

APPENDIX A
DERIVATION OF THE EFFECTIVE THERMAL CONDUCTIVITY FOR FOIL WINDING

In this appendix, the derivation of the equations for the effective conductivity for rectangular and circular foil winding, used in Section II-B3, is explained.

A. XY Rectangular Winding

1) Orthogonal Effective Thermal Conductivity: Considering a plane wall made by several layers of conductor material and other layers of insulator, according to Fig. 6, the total thermal resistance in the orthogonal direction (*X* or *Y*) can be calculated as the series association of the thermal resistance of each layer (see [7] and [8]) by means of the next expression as

$$R_{\text{th}_{\text{ort}}} = \frac{l_{\text{cond}}}{k_{\text{cond}} \cdot A} + \frac{l_{\text{ins}}}{k_{\text{ins}} \cdot A}. \tag{12}$$

Being A the cross section, l_{cond} and l_{ins} the total width of conductor and insulation regions (for Fig. 6: considering the red layers as conductors and yellow ones as insulation, $l_{\text{cond}} = l_1 + l_3$ and $l_{\text{ins}} = l_2 + l_4$); k_{cond} and k_{ins} are their corresponding thermal conductivity.

Now, according to the definition of a thermal resistance, $R_{\text{th}_{\text{ort}}}$ can be expressed in terms of its effective thermal conductivity as

$$R_{\text{th}_{\text{ort}}} = \frac{l_{\text{tot}}}{k_{\text{eq}_{\text{ort}}} \cdot A}. \tag{13}$$

Rearranging this equation, the orthogonal thermal conductivity $k_{\text{eq}_{\text{ort}}}$ can be computed as a function of the thermal conductivity and length of each material region as

$$k_{\text{eq}_{\text{ort}}} = \frac{(l_{\text{cond}} + l_{\text{ins}}) \cdot k_{\text{cond}} \cdot k_{\text{ins}}}{l_{\text{cond}} \cdot k_{\text{ins}} + l_{\text{ins}} \cdot k_{\text{cond}}}. \tag{14}$$

2) Effective Thermal Conductivity in the Vertical Direction: Regarding the analysis of the multilayer plane wall in the vertical direction (*Z*), the corresponding thermal network is the parallel association of the thermal resistance of each region as

$$R_{\text{th}_z} = \left(\frac{1}{R_{\text{th}_{\text{cond}-Z}}} + \frac{1}{R_{\text{th}_{\text{iso}-Z}}} \right)^{-1} = \\ = \left(\frac{k_{\text{cond}} \cdot A_{\text{cond}}}{l_z} + \frac{k_{\text{ins}} \cdot A_{\text{ins}}}{l_z} \right)^{-1}. \tag{15}$$

The previous equation can be defined in terms of its effective conductivity as

$$R_{\text{th}_z} = \frac{l_z}{k_{\text{eq}_z} \cdot A_{\text{tot}_z}}. \tag{16}$$

Following the same concept than in the previous case, and assuming that all regions have the same vertical length (l_z), the effective conductivity in the vertical direction can be described as

$$k_{\text{eq}_z} = \frac{k_{\text{cond}} \cdot A_{\text{cond}} + k_{\text{ins}} \cdot A_{\text{ins}}}{A_{\text{cond}} + A_{\text{ins}}}. \tag{17}$$

B. RZ Circular Winding

In order to define the effective thermal conductivity of a circular winding, the procedure is the same than for the previous section. However, the thermal resistances in this case are expressed in cylindrical coordinates, according to Fig. 7.

1) Effective Radial Thermal Conductivity: In the radial direction, the thermal resistance of each region n is defined as [7], [8]

$$R_{\text{th}_{n-r}} = \frac{ln(r_{n-\text{out}}/r_{n-\text{in}})}{2\pi \cdot l_z \cdot k_n} \tag{18}$$

where $r_{n-\text{out}}$ and $r_{n-\text{in}}$ are the outer and inner radius of the n layer, respectively; l_z is the height of the winding; and k_n is the thermal conductivity of the n layer.

Then, analyzing the circular foil winding in the radial direction, the total radial thermal resistance is equal to the series association of each layer's thermal resistance as

$$R_{\text{th}_r} = \sum_n R_{\text{th}_{n-r}} = \frac{ln(r_{\text{out}}/r_{\text{in}})}{2\pi \cdot l_z \cdot k_{\text{eq}_r}} \tag{19}$$

where r_{out} and r_{in} are the outer and inner radius of the whole winding and k_{eq_r} is the effective thermal conductivity in the radial direction.

Finally, by rearranging the previous equation, k_{eq_r} can be described in terms of the radius and conductivity of each layer as

$$k_{\text{eq}_r} = \frac{ln(r_n/r_1) \cdot k_{\text{cond}} \cdot k_{\text{ins}}}{k_{\text{ins}} \sum_{n_{\text{cond}}} ln(\frac{r_{n+1}}{r_n}) + k_{\text{cond}} \sum_{n_{\text{ins}}} ln(\frac{r_{n+1}}{r_n})}. \tag{20}$$

2) Effective Thermal Conductivity in the Vertical Direction: In both rectangular and circular foil winding cases, (17) is applied.

REFERENCES

[1] *Ferrites and accessories*, TDK, Tokyo, Japan, Appl. Note, May 2017.
[2] *Powder Cores catalog*, Magnetics Inc., Pittsburgh, PA, USA, 2017.
[3] L. M. Escribano, P. Zumel, R. Prieto, J. A. Oliver, and J. A. Cobos, "A very simple analytical approach of thermal modeling for magnetic components," in *Proc. IEEE 20th Annu. Appl. Power Electron. Conf. Expo.*, 2005, vol. 3. pp. 1944–1950.
[4] M. Delhommais, J. Schanen, F. Wurtz, C. Rigaud, C. Sylvain, and S. Vighetti, "Thermal model of litz wire toroidal inductor based on experimental measurements," in *Proc. IEEE Appl. Power Electron. Conf. Expo.*, 2018, pp. 2658–2665.
[5] J. C. Fagundes, A. J. Batista, and P. Viarouge, "Thermal modeling of pot core magnetic components used in high frequency static converters," *IEEE Trans. Magn.*, vol. 33, no. 2, pp. 1710–1713, Mar. 1997.
[6] L. M. Escribano, R. Prieto, J. A. Oliver, J. A. Cobos, and J. Uceda, "Analytical thermal model for magnetic components," in *Proc. IEEE 34th Annu. Power Electron. Specialist Conf.*, 2003, vol. 2, pp. 861–866.
[7] T. L. Bergman, A. S. Lavine, F. P. Incropera, and D. P. Dewitt, *Fundamentals of Heat and Mass Transfer*, 7th ed. New York, NY, USA: Wiley, 2012.
[8] Y. Cengel, *Heat and Mass Transfer: Fundamentals and Applications*. New York, NY, USA: McGraw-Hill, 2014.
[9] K. Pietrak and T. S. Wisniewski, "A review of models for effective thermal conductivity of composite materials," *J. Power Technologies*, vol. 95, no. 1, pp. 14–24, 2015.
[10] F. Chauvicourt, P. Romanazzi, D. Howey, A. Dziechciarz, C. Martis, and C. T. Faria, "Review of multidisciplinary homogenization techniques applied to electric machines," in *Proc. 11th Int. Conf. Ecological Veh. Renewable Energies*, 2016, pp. 1–9.
[11] G. Salinas, A. Delgado, J. A. Oliver, and R. Prieto, "Fast FEA thermal simulation of magnetic components by winding equivalent layers," in *Proc. IEEE Energy Convers. Congr. Expo.*, 2017, pp. 1–120.
[12] Materials catalog. 2018. [Online]. Available: http://www.goodfellow.com/E/Copper.html, Accessed on: Dec. 17, 2018, Goodfellow-Supplier of materials for research and development.
[13] L. Siesing, A. Reinap, and M. Andersson, "Thermal properties on high fill factor electrical windings: Infiltrated vs non infiltrated," in *Proc. Int. Conf. Elect. Mach.*, 2014, pp. 2218–2223.
[14] Z. Hashin and S. Shtrikman, "A variational approach to the theory of the elastic behaviour of multiphase materials," *J. Mechanics Phys. Solids*, vol. 11, no. 2, pp. 127–140, 1963.
[15] N. Simpson, R. Wrobel, and P. H. Mellor, "Estimation of equivalent thermal parameters of impregnated electrical windings," *IEEE Trans. Ind. Appl.*, vol. 49, no. 6, pp. 2505–2515, Nov./Dec. 2013.
[16] M. Jaritz, A. Hillers, and J. Biela, "General analytical model for the thermal resistance of windings made of solid or litz wire," *IEEE Trans. Power Electron.*, vol. 34, no. 1, pp. 668–684, Jan. 2019.
[17] P. A. Kyaw, J. Qiu, and C. R. Sullivan, "Analytical thermal model for inductor and transformer windings and litz wire," in *Proc. IEEE 19th Workshop Control Modeling Power Electron.*, 2018, pp. 1–9.
[18] R. Wrobel, S. Ayat, and J. L. Baker, "Analytical methods for estimating equivalent thermal conductivity in impregnated electrical windings formed using litz wire," in *Proc. IEEE Int. Electric Mach. Drives Conf.*, 2017, pp. 1–8.
[19] C. R. Sullivan, "Prospects for advances in power magnetics," in *Proc. 9th Int. Conf. Integr. Power Electron. Syst.*, 2016, pp. 1–9.
[20] X. Nan and C. R. Sullivan, "An equivalent complex permeability model for litz-wire windings," *IEEE Trans. Ind. Appl.*, vol. 45, no. 2, pp. 854–860, Mar./Apr. 2009.
[21] R. Y. Zhang, J. K. White, J. G. Kassakian, and C. R. Sullivan, "Realistic litz wire characterization using fast numerical simulations," in *Proc. IEEE Appl. Power Electron. Conf. Expo.*, 2014, pp. 738–745.
[22] A. Roßkopf, E. Bär, C. Joffe, and C. Bonse, "Calculation of power losses in litz wire systems by coupling FEM and PEEC method," *IEEE Trans. Power Electron.*, vol. 31, no. 9, pp. 6442–6449, Sep. 2016.
[23] A. Delgado, G. Salinas, J. A. Oliver, J. A. Cobos, J. Rodríguez, and S. Premo, "Equivalent parameters of round and litz wire conductors to obtain an equivalent layer to accelerate finite element simulations of wireless power transfer system," in *Proc. IEEE Energy Convers. Congr. Expo.*, 2018, pp. 7375–7379.
[24] *Thermal Imaging Guidebook for Industrial Applications*, FLIR, Wilsonville, OR, USA, Appl. Note, 2011.
[25] *Thermal Imaging Cameras: A Fast and Reliable Tool for Testing Solar Panels*, FLIR, Wilsonville, OR, USA, Tech. Note, 2007.
[26] *Ti200, Ti300, Ti400 - Thermal Imagers*, FLUKE, Everett, WA, USA, User Manual, 2013.
[27] *Ferrite Materials Survey*, Ferroxcube, Eindhoven, Netherlands, 2008.
[28] The engineering toolbox: Air - thermal conductivity. [Online]. Available: https://www.engineeringtoolbox.com/air-properties-viscosity-conductivity-heat-capacity-d_1509.html [Accessed 01-12-2018]
[29] *Icepak Help Release 2019 R1*, ANSYS Inc., Canonsburg, PA, USA, Jan. 2019.

Guillermo Salinas López received the B.Sc. degree in electronics engineering from the Universidad Miguel Hernández (UMH), Elche, Spain, and the M.Sc. degree in industrial electronics from the Universidad Politécnica de Madrid' (UPM), Madrid, Spain, in 2015 and 2016, respectively. In both universities, he has been enrolled the corresponding power electronics research centers, participating in the design and optimization of power converters for space applications and other R&D projects for important companies of the sector, since 2014.

His current Ph.D. research interests are focused on the thermal modeling of high-frequency magnetic components and its optimization. He carried out a stay as a Visiting Researcher at the European Space Agency.

Alberto Delgado Expósito received the B.Sc. degree in electrical engineering from the University of Málaga (UMA), Málaga, Spain, in 2016, and the M.Sc. degree in industrial electronics from the Universidad Politécnica de Madrid (UPM), Madrid, Spain, in 2017. He is currently working toward the Ph.D. degree in industrial electronics at UPM.

His research activities include modeling of dc–dc converters for inductive power transfer system, magnetic components for different applications such as RFID communications and wireless charging, and magnetic nano-materials and micro-materials.

Mr. Delgado was awarded honors on several occasions and achieved the Best Student of the Year Award during his undergraduate studies.

Javier Muñoz-Antón received the master's and doctoral degrees on mechanical engineering from Universidad Politcnica de Madrid (UPM), Madrid, Spain, in 2005 and 2008, respectively.

He became an Assistant Professor in 2006 and an Associate Professor in 2012. He has been author and co-author in more than 90 scientific paper on journals and conferences and holds 30 patents. He has led several research projects with private and public funding, and he has participated in more than 20 direct R&D projects with companies in Europe. His research interests include heat transfer, thermal engineering, thermal inefficiencies, thermal modeling, CFD, cryogenics, and renewable energy.

Jesús Ángel Oliver Ramírez received the master's and doctoral degrees in electrical engineering from Universidad Politécnica de Madrid (UPM), Madrid, Spain, in 1996 and 2007, respectively.

He became an Assistant Professor in 2001 and an Associate Professor with UPM in 2007. He has been author and co-author in more than 150 scientific papers on journals and conferences and holds five patents. He has led numerous research projects with private and public funding, and he has participated in more than 50 direct R&D projects with companies in Europe, US, Australia, and China. His research activities include modeling (dc–dc converters, magnetic components, piezoelectric transformers, fuel-cells, and dc distributed power electronic systems), fast control techniques for dc–dc converters for VRM applications and RF amplifiers, three-phase rectifiers for aircraft applications, wireless power transfer, and power systems on Chip.

Dr. Oliver is serving as an Associate Editor of the IEEE TRANSACTIONS ON POWER ELECTRONICS.

Roberto Prieto López received the master's and doctoral degrees in electrical engineering from the Universidad Politécnica de Madrid, Madrid, Spain, in 1993 and 1998, respectively.

He is a Full Professor with Universidad Politécnica de Madrid. His contributions are focused on the field of power supply systems for telecom, aerospace, automotive, and medical applications. He has authored or coauthored more than 250 technical papers and holds two patents. He has been actively involved in over 50 research and development projects awarded with public funding in competitive programs, and above 40 direct contracts for research and development for different companies worldwide, including ANSYS, Alcatel, Intel, General Electric, Indra, Siemens, Philips, EADS, and Boeing and Sener. His research interests include magnetic components, modeling, power electronics CAD tools, and modeling of components and systems for power delivery.

Prof. López was a recipient of the UPM Researcher Award for faculty younger than 35 years of age. He has advised six doctoral dissertations and conducted several professional seminars and tutorials.